Proceedings of the 20th International Conference on Soil Mechanics and Geotechnical Engineering– Rahman and Jaksa (Eds)

Numerical approach for predicting large deformation of soil structures using the Convected Particle Domain Interpolation (CPDI) method

Approche numérique pour la prévision de la grande déformation des structures du sol en utilisant la méthode CPDI (Convected Particle Domain Interpolation)

Christian Moormann & Shreyas Giridharan
Institute for Geotechnical Engineering, University of Stuttgart, Germany, christian.moormann@igs.uni-stuttgart.de

Dieter F.E. Stolle
Department of Civil Engineering, McMaster University, Canada

ABSTRACT: Traditional geotechnical analyses carried out for structures involve assessing the onset of failure and designing structures that can sustain loads that they would encounter. Large mass movements are typically avoided. In this work, the Convected Particle Domain Interpolation (CPDI) method, an advancement to the classical Material Point Method (MPM) is utilised to represent the soil structure. The numerical package can simulate and investigate large mass movements should catastrophic damage occur. It can estimate the large deformations encountered in granular media during failure with the aid of an advanced elasto-plastic constitutive law – UBCSAND model. The numerical tool's ability to capture large material movement is highlighted in this paper, in which a granular column collapse is simulated with the predictions compared against experimental results.

RÉSUMÉ : Les analyses géotechniques traditionnelles effectuées pour les structures impliquent l'évaluation du début de la défaillance et la conception des structures de manière à ce qu'elles puissent supporter les charges qu'elles rencontreraient, les grands mouvements de masse étant rarement rencontrés. Dans ce travail, la méthode CPDI (Convected Particle Domain Interpolation), un progrès par rapport à la méthode classique des points de matériaux (MPM), est utilisée pour représenter la structure du sol. Ensemble, le progiciel numérique peut simuler et étudier de grands mouvements de masse lorsque des dommages catastrophiques se produisent sur les structures. L'outil numérique peut estimer les grandes déformations rencontrées dans les milieux granulaires lors d'une défaillance à l'aide d'une loi constitutive élasto-plastique avancée - le modèle UBCSAND, qui est inscrit dans le code. La capacité de l'outil numérique à saisir les grands mouvements de matériaux, qui sont généralement entravés dans les logiciels géotechniques commerciaux, est mise en évidence dans ce travail, et les applications à une simulation d'effondrement de colonne granulaire comparée à des résultats expérimentaux sont utilisées à titre d'exemple.

KEYWORDS: large deformation, CPDI, material point method, granular media, UBCSAND

1 INTRODUCTION

A particularly challenging aspect in the context of finite elements analysis is the modelling of large deformations. Capturing large material movements has been of interest, not only for structural engineering problems but has also found its use in the geotechnical community. There have been a number of approaches developed to capture large deformations, the most popular including: 1) Arbitrary Lagrangian Eulerian method (ALE) (Donea, Huerta, Ponthot, & Rodríguez-Ferran, 2017), 2) Coupled Eulerian Lagrangian method (CEL) (Qiu, Henke, & Grabe, 2011), 3) Particle-In-Cell method (PIC) (Harlow, 1964), 4) Material Point Method (MPM) (Coetzee, Vermeer, & Basson, 2005) to name a few. The Material Point Method (MPM) has gained traction in the past decade due to its versatility in handling contact, soil-structure in interaction and the availability of a plethora of constitutive laws that model soil more accurately. MPM has been improved over the years in the form of the Generalized Interpolation Material Point method (GIMP) (Bardenhagen & Kober, 2004) and the Convected Particle Domain Interpolation method (CPDI) (Sadeghirad, Brannon, & Burghardt, 2011). Improvements in the formulation were effected to improve the performance and accuracy. There have been other conventional methods employed to improve the efficiency of the code, such as adopting higher-order elements or B-Spline functions. A numerical overhead is naturally imposed in such cases. The CPDI variation of the classical MPM is emphasized in this work.

It is important that the numerical implementation is tested and validated. Variables like the sensitivity of a solution to the meshing scheme used (mesh dependency), numerical damping and background smoothening algorithms must be understood to ensure that the simulations not only match the experimental measurements but are also numerically accurate and not a result of numerical artefacts within the code. To this end, this paper aims to outline the theory behind an in-house CPDI code and compares the performance of MPM and CPDI using the Method of Manufactured Solutions, as well as providing results from mesh sensitivity analyses. The predictions of a granular column collapse experiment from a simulation employing the UBCSAND elasto-plastic constitutive law are also provided and compared to the experimental observations.

2 CONVECTED PARTICLE INTERPOLATION METHOD

In the classical formulation of MPM, the continuum is represented by *Lagrangian points* that are commonly referred to as *particles/material points*. The particles move through a fixed *Eulerian* mesh, commonly referred to as *background grid/mesh*.

State variables and physical properties of the continuum such as mass, momentum, stress and strain, as well as other state variables are stored in the particles. At the beginning of a computational step, all relevant information required for the solution is transferred from the particles to the *background computational grid* with the help of suitable shape functions. The incremental solution is determined on the grid in a *Lagrangian* fashion. At the end of the computational step, the solution is mapped back to the particles from the background to update the information residing with the particles, and the grid is reset for the next computational step. The best aspects of *Lagrangian* and *Eulerian* approaches are utilised while avoiding some shortcomings of both. A detailed formulation of MPM is available in Reference (Kafaji, 2013).

One drawback of the classical MPM formulations is the *cell-crossing noise* that causes spurious variations in the internal energy $\boldsymbol{F_{int}}$ that is described by the relation:

$$\boldsymbol{F_{int}} = \boldsymbol{B^T \sigma}, \tag{1}$$

where $\boldsymbol{\sigma}$ the total stress and $\boldsymbol{B}$ represents the strain-displacement matrix. When adopting linear shape functions for the solution process, the gradients are "constant" within each cell, leading to discontinuous values between cells, which in turn causes a jump in the local internal forces as the "collocated" particles migrate from one cell to another. CPDI mitigates this noise by defining a finite size domain, such as that employed in GIMP, allowing the particles to gradually cross boundaries.

As opposed to the classical MPM wherein the particle domains are collocated, the CPDI method defines two vectors (r_1^0, r_2^0), with the superscript *0* representing the current initial state, and the subscripts *1* and *2* referring to two vectors that are originally in the horizontal and vertical directions, respectively. These vectors are used to track the deformation of a particle according to the relations:

$$\boldsymbol{r_1^n} = \boldsymbol{F_p^n}\ \boldsymbol{r_1^0}, \quad \boldsymbol{r_2^n} = \boldsymbol{F_p^n}\ \boldsymbol{r_2^0}, \tag{2}$$

in which *n* refers to the updated time step and $\boldsymbol{F_p^n}$ is the updated deformation gradient. In order to eliminate the need to divide the continuum into particles according to the cell boundaries, an alternate set of shape functions are defined according to the domain of each particle, given by:

$$\phi_{ip} \cong \frac{1}{4}\left[S_i\left(\mathrm{x_1^p}\right) + S_i\left(\mathrm{x_2^p}\right) + S_i\left(\mathrm{x_3^p}\right) + S_i\left(\mathrm{x_4^p}\right)\right], \tag{3}$$

with $S_i\left(\mathrm{x_j^p}\right)$ representing the grid shape functions with $j \in [1,2,3,4]$ referring to corners of particle *p's* domain. The deformation gradient shown in Equation (2) is updated using the relation:

$$F_p^{n+1} = \left(\boldsymbol{I} + \nabla v_p^{n+1}\Delta \mathrm{t}\right)F_p^n, \tag{4}$$

where $\Delta \mathrm{t}$ is the incremental time step and $\boldsymbol{I}$ is the second-order identity tensor. The extension of CPDI to axisymmetric problems is presented in reference (Hamad, 2016), and the extension of axisymmetric problems to accommodate saturated media along with applications is described in reference (Giridharan, Gowda, Stolle, & Moormann, 2020).

2.1 *Performance of MPM and CPDI*

As indicated previously, the assigning of finite-sized domains to the particles avoids the generation of spurious internal forces. The errors associated with these two methods are compared in this section. To this end, the Method of Manufactured Solutions (MMS) is used. The MMS is particularly useful in this case as it provides a procedure to manufacture an exact solution, without being concerned about its physical realism. Analytical solutions can be obtained for code accuracy verification. Readers are directed to Reference (Roache, 2002) for an overview of MMS. The comparison of performance presented in this work is for a two-dimensional problem. Similar tests have been carried out in references (Sadeghirad, Brannon, & Burghardt, 2011), (Sadeghirad, Brannon, & Guilkey, 2013). Since the solution of the model is known *a priori*, the external force required to achieve the desired deformation can be analytically determined. Although the MMS procedure is intended for total *Lagrangian* form, and the current CPDI algorithm utilizes an updated *Lagrangian* form, the solutions are comparable (Wallstedt & Guilkey, 2008).

The external force formulation used in the frame of total *Lagrangian* formulation can be adopted for the current CPDI scheme. A unit square domain (L = 1 m) is assumed and as indicated in reference (Sadeghirad, Brannon, & Burghardt, 2011), the displacement fields are given by the relations:

$$u_x = A\ \sin\left(\frac{2\pi X}{L}\right)\sin\left(\frac{C\pi t}{L}\right), \text{ and}$$

$$u_y = A\ \sin\left(\frac{2\pi Y}{L}\right)\sin\left(\frac{C\pi t}{L} + \pi\right), \tag{5}$$

where, A is the maximum amplitude of 5 cm, X and Y are positions in the reference configuration. Constant C is defined by the relation:

$$C = \sqrt{E/\rho_0}\ . \tag{6}$$

with the modulus of elasticity being $E = 1 \cdot 10^4$ and Poisson's ratio taking on the value 0.3 and the initial density (ρ_0) taken as $1\ g/cm^3$. Substituting Eq. (5) into the equations of motion, in combination with a neo-Hookean law, yields the body forces. A detailed derivation of the body forces are presented in (Sadeghirad, Brannon, & Burghardt, 2011). The comparison between the two methods is achieved by quantifying the error norm calculated from the two methods, which is given by the relation:

$$Error = \frac{\sqrt{\Sigma^{N_t}\Sigma^{N_p}\ ||\Delta \mathbf{u}||^2}}{N_t \times N_p}, \tag{7}$$

where, $\Delta\mathbf{u}$ is the difference between the computed and analytical displacements, N_t and N_p are the total number of time steps and particles, respectively. The problem domain is discretized using five resolutions: 8×8, 16×16, 32×32, 64×64 and 128×128 elements. Each grid element is populated with 1, 4 or 9 particles. Timestep $\Delta t = 0.4\sqrt{\Delta x/C}$, where Δx is the computational grid size. The problem is repeated for classical MPM and CPDI formulations. Figure 1 shows the rate of convergence for the MPM and CPDI methods for the different simulations. A lower rate of convergence is observed in the MPM method compared to that obtained by the CPDI algorithm for each of the cases. This is an indication that the alternative basis functions proposed for the CPDI assist in evaluating the mapping matrix that couples grid values to particles values (ϕ_{ip}), and its gradients $(\nabla\phi_{ip})$ more accurately.

By increasing the number of particles per element while keeping the grid size constant, the error is reduced roughly linearly, although a more pronounced error reduction is noticed in the CPDI method than in the MPM. For the case at hand, regular distribution of particle domains is used. For cases where the region of high particle activity in the form of deformation or strain generations is expected beforehand, a non-uniform particle distribution would be computationally less taxing. Care must, however, be taken to ensure adequate particle packing on the

regions with larger particle distribution to ameliorate build-up of error.

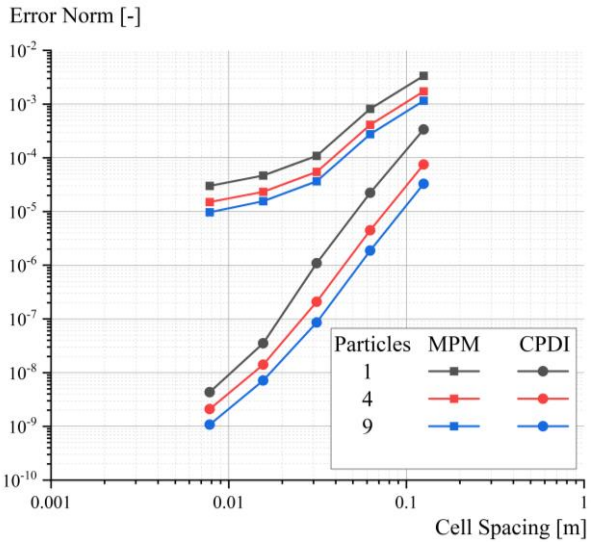

Figure 1. Convergence curves for classical MPM and CPDI method for axis-aligned displacement in a unit square problem.

2.2 *Verification of frame-indifference*

Another important aspect of numerical modelling of large deformations is the principle of material frame indifference. For small deformation problems, a difference between the reference and deformed configuration can normally be neglected when setting up the field equations. This cannot be assumed for finite deformations. The principle of material objectivity requires that the material response be independent of the observer. Thus, constitutive laws must be written in such a manner to obey this. Interested readers are directed to Reference (Malvern, 1969), who provides more information about material frame difference. Reference (Speziale, 1998) also presents a critical review of the concepts of material frame indifference, as does Reference (Belytschko, Liu, Moran, & Elkhodary, 2013), who provide a comprehensive survey of material objectivity in the context of continuum mechanics.

Within the context of MPM, Reference (Kamojjala & Brannon, 2011) present an efficient algorithm using polar decomposition. The algorithm presented in this reference has been implemented in the CPDI code used in this work. The idea behind their algorithm highlights the fact that the approaches commonly used to satisfy objectivity does not suffice. Obtaining solutions assuming an unrotated frame, and implicitly neglecting rotations during the time increment by employing a single orthogonal tensor for all non-rotation operations during the time step might lead to an incorrect solution in finite deformations. The algorithm employed is as follows: 1) stresses $\boldsymbol{\sigma}_n$ are initialized, where *n* is the time; 2) stresses are unrotated using the relation $\bar{\boldsymbol{\sigma}}_n = \boldsymbol{F}_n^T \cdot \boldsymbol{\sigma}_n \cdot \boldsymbol{F}_n$; 3) updated stresses ($\bar{\boldsymbol{\sigma}}_{n+1}$) are then computed using a suitable constitutive law; and 4) updated unrotated stresses are rotated back using the relation $\boldsymbol{\sigma}_{n+1} = \boldsymbol{F}_{n+1}^T \cdot \bar{\boldsymbol{\sigma}}_{n+1} \cdot \boldsymbol{F}_{n+1}$. The same algorithm can be employed for the symmetric part of the velocity gradient $\boldsymbol{D}_n$. For the sake of completeness, it is to be noted that the incorrect way of performing this procedure is to use a constant deformation gradient $\boldsymbol{F}_n$ without updating it.

To demonstrate the algorithm, a classical unit square element test is performed using CPDI. The solution consists of two stages: 1) uniaxial straining, where the acceleration due to gravity acts on the element, increasing its stress from 0 to its maximum value; and then 2) the rigid body rotation of the element is introduced, which is achieved by slowly rotating the block by 90°. The entire simulating takes place in 2 seconds, each phase taking a second. As an example for this simulation, a linear elastic constitutive law is chosen with the modulus of elasticity as 500 *kPa* and Poisson's ratio as 0.3. An explicit time-stepping algorithm is employed. From Fig. 2, it can be inferred that the vertical and horizontal stresses increase linearly during the first phase of the solution. In the second phase, the gravity vector is rotated by 90°, to simulate the rotation of the block. The horizontal and vertical stress swap values with each other, as one would expect. Small shear stresses that are generated quickly dissipate as the solution progresses. Results from this test conclusively prove that regardless of large rotations, objectivity criterion is satisfied in the numerical code.

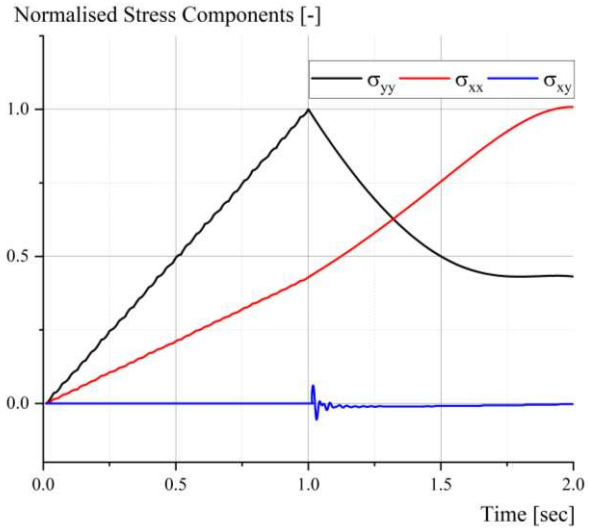

Figure 2. Normalized stress components vs. time for rotated block simulation.

3 GRANULAR COLUMN COLLAPSE

The CPDI code that is presented and tested in Section 2 is now used to simulate the collapse of a granular column, in which the predictions are compared with the experimental results. The goal is to examine the influence of variables such as particles per cell, numerical damping, and the effects of the smoothening algorithm and constitutive law. The simulation of granular column collapse is not new, having been already published in References (Kermani, Li, & Qiu, 2014), (Kumar, Delenne, & Soga, 2017), (Mast, Arduino, Mackenzie-Helnwein, & Miller, 2015). Reference (Sołowski & Sloan, 2013) performed a granular column collapse study using MPM. Numerical damping was introduced into the simulation to obtain a better fit to the result, as higher-than-expected run-off was observed for columns with high aspect ratios (greater than 2.0). Efforts have been made in the current study to gauge the effect of numerical damping on the final-run off, as well as the effect of the number of particles per cell, the effect of smoothening, as well as the effect of constitutive laws on the system. To this end, the experiments performed in Reference (Lube, Huppert, Sparks, & Freundt, 2007) is simulated.

They investigated a two-dimensional granular flow formed during the collapse of a rectangular column of sand into a wide horizontal channel. While different aspect ratios were chosen for the experiments (between 3.0 and 9.5), only corresponding to an aspect ratio of 7.0 is analysed herein. Their container accommodated the granular media at one end of the tank and included a gate to release the granular material. This allowed a more focused parameter study. The width of the column was 9.05 cm, with the height of the column being 63.35 cm. A mixture of industrial black and light grey coloured quartz sands with grain size 1.4 ± 0.4 mm was chosen. The following physical properties

were recorded for the quartz sand: solid density 2650 kg/m^3 and angle of repose 31°. In the experiment, the retaining gates were removed very quickly and the ensuing deformation and the free surface was observed through the glass walls.

Table 1. Parameters for Quartz sand

Parameter	ρ_0 [kg/m^3]	E [kPa]	ν [-]	ϕ [°]	ψ [°]
Value	2650	840	0.3	31	1

An elasto-plastic Mohr-Coulomb failure criterion was chosen in the current study to model the sand, which was replaced with the UBCSAND model. Parameters for the Mohr-Coulomb model are provided in Table 1. A non-slip condition between the granular media and the ground was assigned following Reference (Lube, Huppert, Sparks, & Freundt, 2005). The collapse of the granular column was entirely modelled using CPDI. A two-dimensional regular mesh with a cell dimension of 0.67 mm was chosen. The elements were initially populated with either 1, 4 or 9 particles.

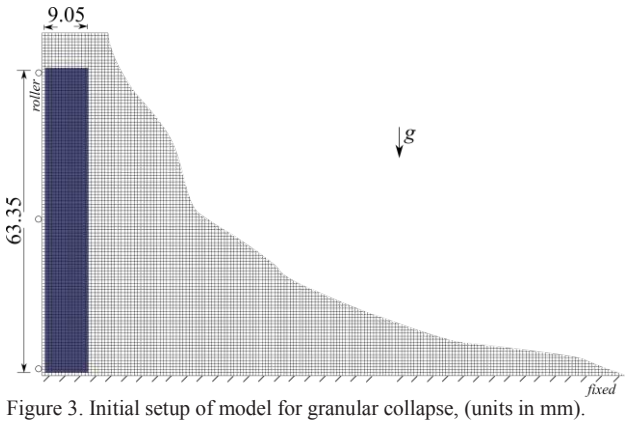

Figure 3. Initial setup of model for granular collapse, (units in mm).

The initial configuration of the simulation is shown in Figure 3, with the computational grid shown in the background and particles being shown in blue. Acceleration due to gravity was taken to be 10 m/s^2. Results from Reference (Lube, Huppert, Sparks, & Freundt, 2007) were digitized to allow for comparison between the simulation and experimental results. Three aspects were studied: 1) effect of the number of particles on the final solution; 2) influence of numerical damping; and 3) effect of kinematic locking smoothening on the final runout. The results of MPM, and by extension, CPDI depend on the mesh. Final results are not only sensitive to the size of the background grid but also to the number of particles that populate the background grid. A parameter study for a dynamic solution in this regard was considered valuable. The influence of numerical damping, often used to assist in convergence, was studied first. Thereafter, the numerical results were compared against a simulation implementing the more advanced, elasto-plastic UBCSAND constitutive law.

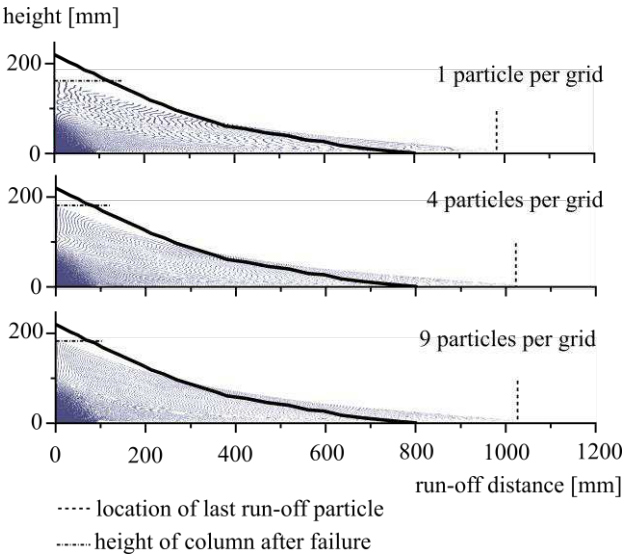

Figure 4. Effect of number of particles on the total run-off.

Figure 4 shows the results of a parameter study where the number of particles per grid was varied between 1 and 9. No numerical damping was used. The background grid was not altered. Results show that regardless of the number of particles, the final run-off is overpredicted in the numerical model. Since the CPDI particles are themselves allowed to deform, it is not surprising to note that different final heights are obtained from the simulation. For the case of 1 particle-per-grid, the run-off is overpredicted and the final height is underpredicted, the latter owing to deformation of the particle. As the number of particles per grid increases, the final height reaches roughly the experimental value. From Figure 1, where there is evidence that a system with higher particles yields lower global error, a choice was subsequently made to perform further simulations with only 9 particles per cell.

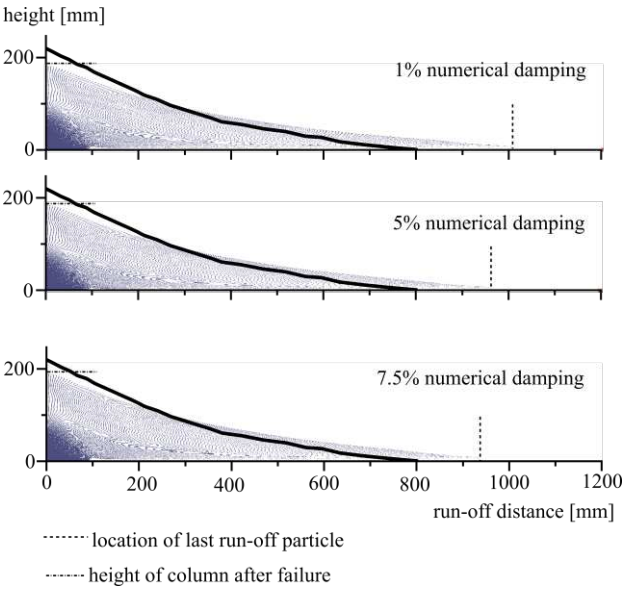

Figure 5. Effect of numerical damping on the total run-off.

Effect of numerical damping is considered next. Reference (Sołowski & Sloan, 2015) had utilised numerical damping for MPM simulations of granular column collapse, in part to improve convergence, and to approximate the loss of energy of grains upon movement without strain change, which is mostly in the form of friction between particles. It is imperative to note that such damping algorithms are artificial in nature, and can

influence the results significantly when used incorrectly. From Figure 5, it can be seen that as the damping coefficient is increased, the final run-off approaches closer to the experimental value, which is similar to what others have experienced.

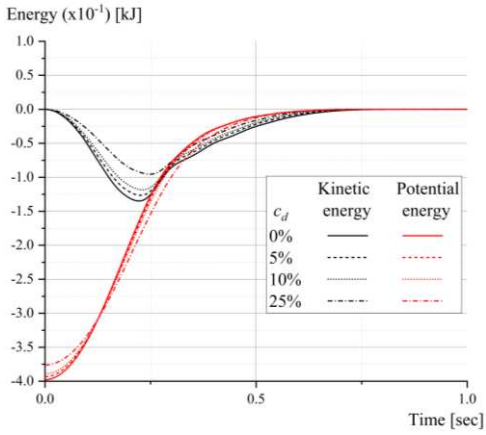

Figure 6. Study of kinetic and potential energies of the system for different damping coefficients.

The kinetic and potential energies of the system for different damping coefficients are presented in Figure 6. While there are no discernible changes observed in the potential energy, as it should be, with minor deviations being considered as a numerical artefact of the solution procedure, kinetic energies show a marked change when damping coefficients are changed. Results from 3D-DEM (Discrete Element Method) simulations performed in Reference (Utili, Zhao, & Houlsby, 2015) for the collapse of a granular column, wherein energy dissipation studies were performed, also drew similar results to those shown in Figure 6, that the loss of energy in the system, owing to intergranular friction, is in the form of kinetic energy.

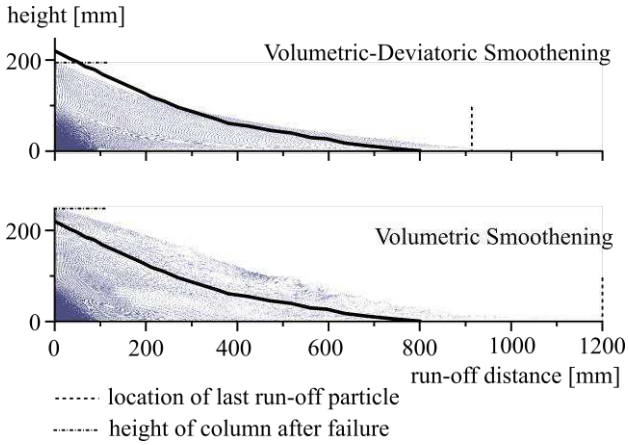

Figure 7. Effect of smoothening on the final run-off.

The effect of locking is especially pronounced when using lower-order elements, like in the case of this work. There are various ways to mitigate the effects of locking in MPM. In some cases undesirable changes in stiffness to the element develop. Readers are directed to Reference (Mast, Mackenzie-Helnwein, Arduino, Miller, & Shin, 2012) for a detailed formulation of the *Hu-Washizu* kinematic locking mitigation algorithm, which served as the basis for the implementation in this CPDI code.

Figure 7 shows the result of using two anti-locking procedures for the granular flow problem. No damping was used for these simulations. We observe that volumetric smoothening yields incorrect results. The run-off is over-predicted, as is the height of the slope. The apparent 'softening' of the material, although beneficial in fluid dynamics problems, where there is increased stiffness in the element due to locking, which is not ideal for granular problems, where the pressure locking effect is less pronounced. On the other hand, the use of deviatoric strain-rate smoothening, which acts on the deviatoric portion of the stress and strain field yields better results. The spurious stress deviations, which are caused in part due to shear locking, is alleviated, and the artificially high run-off, like those observed in Reference (Sołowski & Sloan, 2013) can be reduced. Although a more thorough analysis is required, a theory that is proposed to better the results is that the velocities that are calculated on the grid are a result of the collocated values of stresses and strains from the particles, which are 9 in this case. An averaging exercise happens on the grid, which does not necessarily have the correct value, and leads to an overestimation of the grid, and consequently, the particle velocity. By using a smoothening filter, this error is negated, and the resultant solution is closer to the experimental values.

Reference (Mast C. M., 2013) studied the influence of different failure laws on the final result for the granular column collapse simulation. Reference (Fern & Soga, 2016) also studied the variation in behaviour of granular column collapse using an advanced constitutive law (Nor-Sand) and compared its results with those obtained with the classical Mohr-Coulomb model. This study adopted the UBCSAND constitutive law to model the collapse and make observations about the final run-off. A concise summary of the UBCSAND model is available in Reference (Giridharan, Gowda, Stolle, & Moormann, 2020). Although it is pertinent to note that UBCSAND model is widely used in the field of seismic modelling, and its use here might not be of great value, especially given that the model neither has any appreciable cyclic loads nor is the soil saturated, it is nevertheless of interest to observe the influence of hardening on the final result. This exercise is viewed mainly as an additional validation of not only the CPDI code but also in the in-house implementation of the UBCSAND model, which is based on the work from Reference (Naesgaard, 2011). The parameters for the UBCSAND model, tabulated in Table 2, were calibrated for the quartz sand mixture used in the experiment.

Table 2. Parameters for UBCSAND model

$N1_{60}$[-]	m_e [-]	n_e [-]	n_p [-]	K_G^E [-]	K_B^E [-]
10.7	0.7	0.7	0.4	100	125
K_G^P [-]	ϕ_{pt} [°]	ϕ_f [°]	c [kPa]	Pa [kPa]	σ_t [kPa]
5	31	31.1	0	100	0
$hfac_1$[-]	$hfac_2$[-]	$hfac_3$[-]	$hfac_4$[-]	$hfac_5$[-]	$hfac_6$[-]
0.65	0.85	1.0	0.6	1.0	0.95

Results of the simulation (shown in Figure 8) were obtained with deviatoric smoothening together 5% damping using the Mohr-Coulomb model (represented with a red line) and the UBCSAND model. While the UBCSAND model closely follows the experiments during the first 0.17 seconds, the results start to follow the Mohr-Coulomb model in the latter part of the simulation. The final run-off prediction from both the models are quite close to the result obtained from the experiment (shown in black). The result from the UBCSAND model indicates that the model was marginally stiffer than its Mohr-Coulomb counterpart. One explanation that can be provided for this phenomenon is the presence of a hardening in the case of UBCSAND, in addition to Mohr-Coulomb plasticity correction. This correction is particularly useful in case of modelling liquefaction (Giridharan, Gowda, Stolle, & Moormann, 2020), however in this case, it alters the stiffness too much. A better fit can be obtained by better calibrating the parameters, particularly the hardening factors (*hfac*-s). That would require good quality experimental data, that was in dearth for the quartz sand. Nevertheless, even a cursory calibration procedure was sufficient to achieve reasonable numerical performance from the UBCSAND model, as evidenced by the results presented.

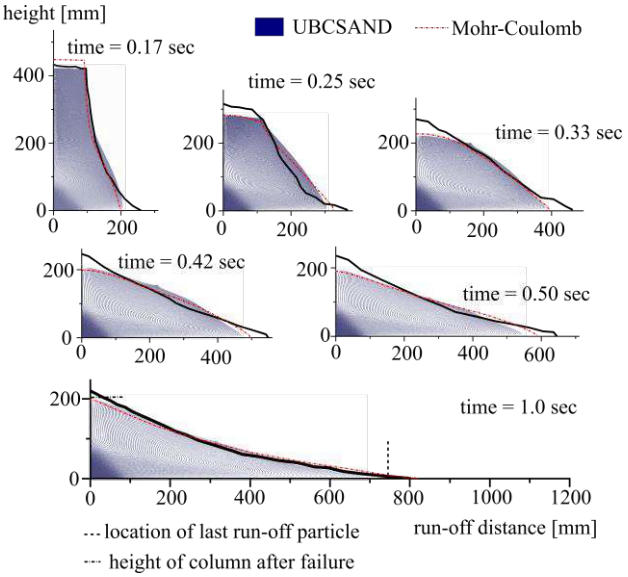

Figure 8. Comparison between simulations performed using Mohr-Coulomb model and UBCSAND constitutive law.

4 CONCLUSIONS

A novel extension of the MPM, known as CPDI towards applications in the field of geotechnical engineering was considered in this study. The aim was to validate the CPDI code, by means of comparing its performance against the classical MPM, and to ensure that the code obeyed the fundamental law of objectivity, which can be overlooked quite easily when implementing the code from a classical finite-element point of view. A granular column collapse simulation was performed and compared against the experimental results, with observations about the effect of various parameters that influence the results made along the way. An advanced elasto-plastic model UBCSAND was used to compare the results against Mohr-Coulomb, yielding comparable results. The CPDI code developed here, although imposes a bit of computational overhead, makes up in the fact that the results from the simulation are more accurate and consequently, can be applied with confidence to real-world problems. Further research in this direction would not only involve dynamic problems like earthquake simulation in saturated sand but also would involve problems involving large time scales, like that of a creeping soil problem.

5 REFERENCES

Bardenhagen, S. G., & Kober, E. M. (2004). The generalized interpolation material point method. Computer Modeling in Engineering and Sciences, 5, 477–496.

Belytschko, T., Liu, W. K., Moran, B., & Elkhodary, K. (2013). Nonlinear finite elements for continua and structures. John Wiley & sons.

Coetzee, C. J., Vermeer, P. A., & Basson, A. H. (2005). The modelling of anchors using the material point method. International journal for numerical and analytical methods in geomechanics, 29, 879–895.

Donea, J., Huerta, A., Ponthot, J.-P., & Rodríguez-Ferran, A. (2017). Arbitrary Lagrangian–Eulerian Methods. Encyclopedia of Computational Mechanics Second Edition, 1–23.

Fern, E. J., & Soga, K. (2016). The role of constitutive models in MPM simulations of granular column collapses. Acta Geotechnica, 11, 659–678.

Giridharan, S., Gowda, S., Stolle, D. F., & Moormann, C. (2020). Comparison of UBCSAND and Hypoplastic soil model predictions using the Material Point Method. Soils and Foundations, 60, 989–1000.

Hamad, F. (2016). Formulation of the axisymmetric CPDI with application to pile driving in sand. Computers and Geotechnics, 74, 141–150.

Harlow, F. H. (1964). The particle-in-cell computing method for fluid dynamics. Methods Comput. Phys., 3, 319–343.

Kafaji, I. K. (2013). Formulation of a dynamic material point method (MPM) for Geomechanical Problems. Ph.D.-Thesis, University of Stuttgart, Institute for Geotechnical Engineering

Kamojjala, K., & Brannon, R. M. (2011). Verification of frame indifference for complicated numerical constitutive models. ASME early career technical conference.

Kermani, E., Li, T., & Qiu, T. (2014). Discrete element method simulation of granular column collapse. In Advances in Transportation Geotechnics and Materials for Sustainable Infrastructure (S. 1–8).

Kumar, K., Delenne, J.-Y., & Soga, K. (2017). Mechanics of granular column collapse in fluid at varying slope angles. Journal of Hydrodynamics, 29, 529–541.

Lube, G., Huppert, H. E., Sparks, R. S., & Freundt, A. (2005). Collapses of two-dimensional granular columns. Physical Review E, 72, 041301.

Lube, G., Huppert, H. E., Sparks, R. S., & Freundt, A. (2007). Static and flowing regions in granular collapses down channels. Physics of Fluids, 19, 043301.

Malvern, L. E. (1969). Introduction to the Mechanics of a Continuous Medium, (no Monograph).

Mast, C. M. (2013). Modeling landslide-induced flow interactions with structures using the material point method. Ph.D. dissertation.

Mast, C. M., Arduino, P., Mackenzie-Helnwein, P., & Miller, G. R. (2015). Simulating granular column collapse using the material point method. Acta Geotechnica, 10, 101–116.

Mast, C. M., Mackenzie-Helnwein, P., Arduino, P., Miller, G. R., & Shin, W. (2012). Mitigating kinematic locking in the material point method. Journal of Computational Physics, 231, 5351–5373.

Naesgaard, E. (2011). A hybrid effective stress–total stress procedure for analyzing soil embankments subjected to potential liquefaction and flow. Ph.D. dissertation, University of British Columbia.

Qiu, G., Henke, S., & Grabe, J. (2011). Application of a Coupled Eulerian–Lagrangian approach on geomechanical problems involving large deformations. Computers and Geotechnics, 38, 30–39.

Roache, P. J. (2002). Code verification by the method of manufactured solutions. J. Fluids Eng., 124, 4–10.

Sadeghirad, A., Brannon, R. M., & Burghardt, J. (2011). A convected particle domain interpolation technique to extend applicability of the material point method for problems involving massive deformations. International Journal for numerical methods in Engineering, 86, 1435–1456.

Sadeghirad, A., Brannon, R. M., & Guilkey, J. E. (2013). Second-order convected particle domain interpolation (CPDI2) with enrichment for weak discontinuities at material interfaces. International Journal for numerical methods in Engineering, 95, 928–952.

Sołowski, W. T., & Sloan, S. W. (2013). Modelling of sand column collapse with material point method. Proceedings of the 3rd international symposium on computational geomechanics (ComGeo III), (S. 698–705).

Sołowski, W. T., & Sloan, S. W. (2015). Evaluation of material point method for use in geotechnics. International Journal for Numerical and Analytical Methods in Geomechanics, 39, 685–701.

Speziale, C. G. (1998). A review of material frame-indifference in mechanics. 489-504.

Utili, S., Zhao, T., & Houlsby, G. T. (2015). 3D DEM investigation of granular column collapse: evaluation of debris motion and its destructive power. Engineering geology, 186, 3–16.

Wallstedt, P. C., & Guilkey, J. E. (2008). An evaluation of explicit time integration schemes for use with the generalized interpolation material point method. Journal of Computational Physics, 227, 9628–9642.